Effect of Surface Topography and Hydrophobicity on Water Entropy

A Thesis
submitted towards the partial fullfilment of
MSc. Degree Programme
by

Mansi Jain

Indian Institute of Science Education and Research Pune
Dr. Homi Bhabha Road,
Pashan, Pune 411008, INDIA.

April, 2024

Supervisor: Prof. Arnab Mukherjee

Certificate

This is to certify that this dissertation entitled Effect of Surface Topography and Hydrophobicity on Water Entropy submitted towards the partial fulfillment of the MSc degree at the Indian Institute of Science Education and Research, represents original research carried out by Mansi Jain at Indian Institute of Science Education and Research, under the supervision of Prof. Arnab Mukherjee during academic year 2023 to 2024.

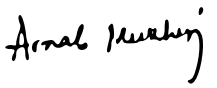

Arnab Mukherjee

This thesis is dedicated to Prof. Arnab Mukherjee and all my lab mates.

Declaration

I, hereby declare that the matter embodied in the report titled Effect of Surface Topography and Hydrophobicity on Water Entropy is the results of the investigations carried out by me at the Indian Institute of Science Education and Research from the period 2023 to 2024 under the supervision of Prof. Arnab Mukherjee and the same has not been submitted elsewhere for any other degree. Wherever others contribute, every effort is made to indicate this clearly, with due reference to the literature and acknowledgement of collaborative research and discussions.

Mansi Jain

Acknowledgements

I would like to express my sincere gratitude to **Prof. Arnab Mukherjee**, my research supervisor, for his support and guidance throughout my project. He has always encouraged me to explore my research topic scientifically and freely while accepting my mistakes along the way. His enthusiasm and dedication to research have inspired me a lot. I would also like to thank **Dr. Srabanti Chaudhury**, my expert, for her valuable insights into my project work.

I would also like to acknowledge the contributions of **Wilbee D. Sasikala**, who originally developed the single water entropy program, and **Debasis Saha**, for modeling one set of my systems. I would like to extend a special thanks to my mentor, **Ashish Kumar**, for his diligence, trust, and guidance, which has been instrumental in my progress. His continuous support has been crucial, from explaining basic methodologies to understanding the topic in depth. Collaborating with him has been a gratifying experience, marked by productive discussions. I am grateful to **Bikirna Roy** for his insightful suggestions during various stages of my research and to **Sarathchandran J.**, a former lab member, for his assistance during my early days in the lab. I would also like to acknowledge Sarathchandran J. for the figure depicting Permutation Reduction that I have utilized. I would also like to thank all current and former members of my lab, including **Amal Vijay, Rahul Hooda, Sonali Jadhav, Uddipan Bhattacharya, Parth Joshi, Prathith Bhargav, Pratishruti Panda, Shreyas Adhury, and Snehash Behera** for their interest and encouragement.

I would like to acknowledge the Indian Institute of Science Education and Research, Pune, for providing the computational facilities, particularly the HPC like **Param Brahma**, which made my simulations faster.

Lastly, I would like to thank my father, **Sushil Panchori**, mother, **Rekha Jain**, brother, **Shalin Panchori**, and all my dear friends for their unwavering emotional support throughout this journey.

Abstract

The entropy of water molecules plays a dominant role in various biological processes, like protein folding and molecular recognition. Understanding the dependence of water entropy on the surface topography and chemistry of biomolecular surfaces is necessary to comprehend these processes. However, calculating water entropy from molecular dynamics simulation remains challenging due to the difficulty in sampling the large phase space, even for a small system of water molecules within realistic time scales. Here, we use the Single Water Entropy (SWE) approach to calculate water entropy, which utilizes Permutation Reduction (PR) to reduce the phase space volume accessible to water. The initial work involved the calculation of water entropy around homogeneous hydrophobic model surfaces. Subsequently, our work was extended to incorporate chemistry in our systems. We also calculated the dynamical properties of water molecules like velocity and rotational autocorrelation functions.

Contents

List of Figures

List of Tables

Chapter 1

Introduction

Water plays a dominant role in the structuring, dynamics, and functionality of biological molecules. A wide range of biophysical processes, like protein folding, protein-ligand binding, and lipid bilayer formation [1–3], are driven by the hydrophobic effect (HE). HE emerges from a balance between the entropy and enthalpy of the first few hydration layers surrounding the biological molecules, making it essential to understand the thermodynamics of the solvation shell in order to gain a better understanding of these processes.

In thermodynamic terms, it is Gibbs free energy ($\Delta G = \Delta H - T\Delta S$) in an isothermal-isobaric ensemble that governs the spontaneity of a process. Understanding the interplay between entropy and enthalpy is useful to comprehend the process at the atomic or molecular level, even though ΔG drives it. Usually, we are interested in the difference in enthalpy between two systems. For incompressible systems at constant pressure, this can be readily obtained by looking at differences in potential energy. Entropy is related to atomic fluctuations, whose quantification is often challenging, especially for complex systems like biological macromolecules and highly diffusive liquids like water. This difficulty in entropy calculations arises because biological macromolecules have large degrees of freedom, and diffusive liquids like water can access a large configuration space volume.

The entropy of water molecules within the biomolecular interface has intricate dependencies on its size, topography, and polarity. Studying the water entropy around homogeneous hydrophobic model surfaces provides a simplified framework, which may serve as a basis for understanding more complex situations, such as hydration water surrounding proteins, where additional factors like polarity and positions of the chemical groups also come into play.

Several studies have investigated the role of surface geometry and polarity on water entropy. For instance, around smaller and hydrophobic spherical solutes, water forms

a clathrate-like water arrangement, leading to a loss in entropy, whereas, around larger solutes, a loosely hydrogen-bonded arrangement prevails [4, 5]. A crossover in entropy behavior was observed. For graphitic sheets, an increase in the thickness of the sheet results in water stabilization within the interface, with entropy playing an essential role in stabilization [6]. Moreover, a decrease in entropy has been observed for water molecules in the first hydration shell with increasing the charge of the ions [7].

Various methods have been used to calculate water entropy in the hydration shell. Estimating entropic contributions to the hydration can be done using methods based on the free energy of transfer between two phases. However, these methods estimate it indirectly by considering the difference between free energy and enthalpy. Thus, a detailed understanding of the entropic effects might not be reached. Traditional methods like thermodynamic integration [8] are also used but lack spatial resolution. Spatially resolved picture of solvent thermodynamics can be obtained using methods like inhomogeneous solvation theory (IST) [9], two-phase thermodynamics(2PT) [10], the spatially resolved (grid-based) extension 3D-2PT [11], a three-dimensional (3D) grid-based adaptation (GIST) [12], and Per|Mut [13].

Since individual water molecules within the hydration shell contribute to the overall water entropy, addressing the entropy of each water molecule becomes crucial. Even the entropy of a single water molecule can impact the free energy of biophysical processes. Thus, our study focuses on calculating single water molecule entropy using a method developed within our group [14].

We initiated our work by calculating water entropy near model surfaces-inside the cavity of varying depths and around hydrophobic sheets with different curvatures. Specifically, we have analyzed the influence of cavity depth and curvature on hydrophobic slabs and sheets, respectively. We then extended our study to incorporate chemical considerations by studying water entropy around graphene-like sheets. Thus, we have examined the effect of hydrophobicity by varying its interaction potential and the effect of surface topography by varying its curvature values. Our study involved computing single water translational and rotational entropy around these surfaces as a function of their average distance. The entropy value inside the cavity was explained using interaction energy. The entropy around the hydrophobic and graphene-like sheets was compared with the dynamical properties, like velocity autocorrelation functions (VACFs) and rotational autocorrelation functions for water within the interface.

Chapter 2

Theory

2.1 Molecular Dynamics Simulations

A Molecular dynamics simulation is a computer simulation that can predict the positions and velocities of a system of particles over time, thereby generating a trajectory. In md simulations, the system is treated classically. An initial model of the system is obtained from experimental techniques such as NMR, crystallographic, or homology modeling. Newton's law of motion calculates the forces acting on every atom at each time interval. At each time step, forces on every atom are calculated, and then the spatial position and velocity of each atom over time are obtained. The forces in md simulations are calculated using molecular mechanical force fields obtained from Quantum-mechanical calculations and certain experimental measurements.

$$\mathbf{F}_i = -\nabla_i V(\mathbf{X}_1, \ldots, \mathbf{X}_n) = m_i \frac{d^2\mathbf{X}_i}{dt^2} = m_i \mathbf{a}_i(t) \tag{2.1}$$

where $\mathbf{X}_i$ represents the position of the ith atom, and V denotes the potential energy due to the non-bonding and bonding interactions between atoms.

2.2 Single Water Entropy

For the calculation of single water entropy, we have used single water entropy (SWE) approach, a method developed within our group [14], which involves reduction of the configurational space volume of water first Permutation Reduction. Then, a quasiharmonic approximation on each permuted water molecule is applied.

2.2.1 Permutation Reduction

The estimation of water entropy is not straightforward. Because of the diffusive nature of water molecules, their configurational phase space volume is too large to be sampled by current simulation techniques. Their configurational phase space density is also complex to be fitted by Gaussian density approximations. Therefore, methods such as quasiharmonic approximations [15], usually used for entropy calculations of biomolecules, cannot be directly used here. To overcome these difficulties, the method of permutation of solvent molecules, as suggested by Grubmüller *et al.* [16] is utilized.

Permutation Reduction (PR) involves the relabelling of the indices of solvent molecules for each trajectory frame x(t) such that the root mean square deviation (rmsd) between the reference configuration and the permuted configuration is minimized. The rmsd is given as:

$$\sum_{i=1}^{N} ||x_{\pi(i)}(t) - r_i||^2 \tag{2.2}$$

where r_i is the reference configuration and $\pi(i)$ is chosen to map the configuration of each frame $x(t)$ to a new configuration which is close to the reference structure.

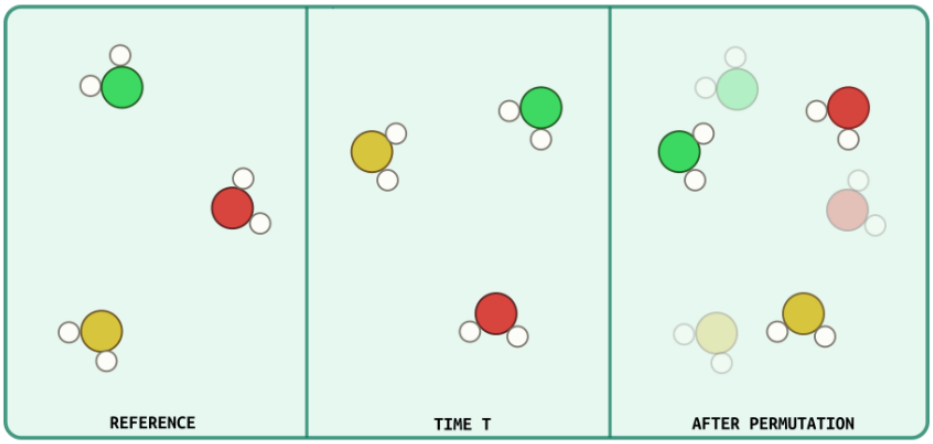

Figure 2.1: The First panel represents a reference frame, the second panel represents a frame at time t, and the third panel represents the relabelling of the molecules based on the proximity to the molecules in the reference frame. Here, the relabelling of the molecules is presented as recoloring.

In this work, each water molecule is permuted separately using asymmetric permutation. So, each permuted water molecule moves only in a localized region and occupies a different configurational volume with minimal overlap. Further, this permuted trajectory is used for entropy calculations.

2.2.2 Entropy Estimation

Translational Entropy

The translational entropy of permuted water molecules can be approximated using quasi-harmonic approximation. Within this approximation, the phase space density of the trajectory x(t) is approximated by a multivariate Gaussian distribution. This distribution is given by:

$$\tilde{\rho}(x) = \frac{1}{\sqrt{(2\pi)^{3N}\det(C)}} e^{-(x-\langle x\rangle)^T C^{-1}(x-\langle x\rangle)} \tag{2.3}$$

where C is a 3 × 3 covariance matrix calculated as:

$$C_{ij} = \langle (x_i - \langle x_i\rangle)(x_j - \langle x_j\rangle)\rangle \tag{2.4}$$

A 3 × 3 covariance matrix of each particle is created, which corresponds to their translational fluctuations along the x,y, and z directions. The eigenvalues (λ_i, i=1-3, obtained by diagonalisation of covariance matrix) of each covariance matrix corresponds to the lengths of the principal axes of the ellipsoid formed by the permuted water molecule. These eigenvalues are used to compute the corresponding frequency:

$$\omega_i = \sqrt{k_B T/\lambda_i} (i = 1 - 3) \tag{2.5}$$

Finally, translational entropy is calculated using the following equation:

$$S_{tr}^{QH} = k_B \sum_{i=1}^{3} \frac{\hbar\omega_i}{k_B T(e^{\frac{\hbar\omega_i}{k_B T}} - 1)} - \ln\left(1 - e^{\frac{-\hbar\omega_i}{k_B T}}\right) \tag{2.6}$$

where, $\hbar$ = h/2π is the plank constant, T is temperature and k_B is the Boltzmann's constant.

The anharmonic contribution has been considered in the entropy calculations by using a method based on kth nearest neighbor distances, following Numata *et al.* [17]

Rotational Entropy

The standard equation of entropy based on the angular distribution of individual permuted water molecules can be used to calculate the rotational entropy. The equation used to calculate rotational entropy [18] is given:

$$S_{rot} = -k_B \int p\left(\theta, \chi\right) c \ln \left\{p\left(\theta, \chi\right) c\right\} \sin \tag{2.7}$$

where $p\left(\theta, \chi\right)$ is the angular distribution of a single water molecule, θ is the angle between the dipole vector and water oxygen to reference particle vector, and χ is defined as the angle between the vector joining the 2 hydrogens of water and the normal to the plane defined by the reference particle-oxygen vector and the dipole vector.

2.2.3 Autocorrelation Functions

Velocity Autocorrelation Function

Diffusion coefficients of the water molecule can be calculated using the velocity autocorrelation function using the Green-Kubo equation [19–21]:

$$D = \frac{1}{d} \int_0^\infty C(t) dt \tag{2.8}$$

where D is the diffusion coefficient, d is the dimensionality and C(t) is the velocity autocorrelation function given by:

$$C(t) = \langle \vec{v}(t) \cdot \vec{v}(0) \rangle \tag{2.9}$$

Rotational Autocorrelation Function

The rotational autocorrelation function for water molecules is computed by averaging the autocorrelation of vectors perpendicular to each water molecular plane. $\mathrm{C(t)}_{rot}$ is the rotational autocorrelation function given by:

$$C(t)_{rot} = \langle \vec{u}(t) \cdot \vec{u}(0) \rangle \tag{2.10}$$

where $\vec{u}$ is defined as the unit vector perpendicular to the plane of a water molecule at time t.

2.2.4 Proximal Radial Distribution Function

The proximal radial distribution function calculates the probability of finding the solvent molecules at distance r from the surface of solute. It gives the number density of solvent molecules as a function of the distance from the nearest atom of the solute. The coordination number of the solvent atoms in the available volume N(r) and the available volume V(r) with thickness Δ r (at a distance r from the nearest solute atom) are computed in this function. Numerical density of the solvent ρ(r) = N(r)/V(r).

Chapter 3

Methods

3.1 System Preparation

The construction of the three sets of systems that we have studied is described below:

3.1.1 Slabs with Hydrophobic Cavity

We have constructed a slab of neutral particles aligned in a hexagonal close-packed (hcp) grid with a lattice constant of 1.25 Å. The cavity was constructed by deleting all the atoms within a given volume from a central atom at the slab's surface. Two systems with the conical cavity of the same volume but depth of 5 and 10 Å were studied.

The 5 and 10 Å slabs were solvated with 5251 and 5291 water molecules, respectively. SPC/E water model [22] was used for solvation. The attractions between water and the surface were considered weak to mimic a hydrophobic system. Hence, Lennard-Jones (LJ) parameter $\epsilon = 0.478$ kJ mol^{-1} and $\sigma = 0.3275$ nm were used for the atomic species of these surfaces. The slabs were placed at the center of the box and parallel to the xy plane. The conical cavity lies along the z-axis.

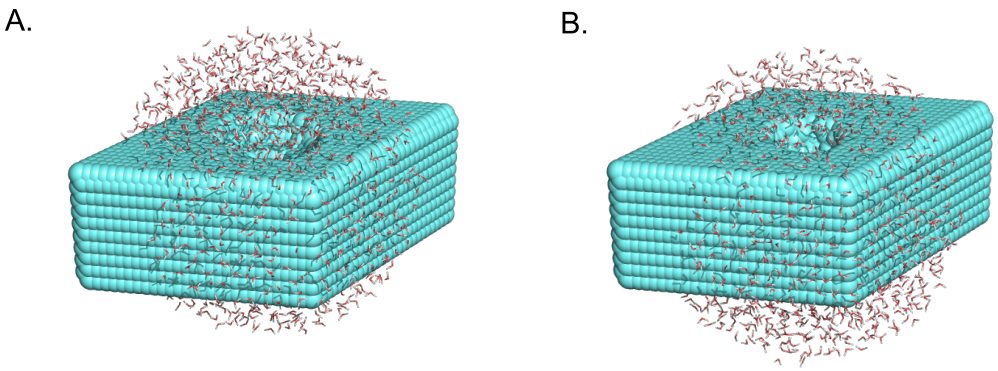

Figure 3.1: Hydrophobic slabs with cavities of depths 6 (A) and 10 (B) Å in water. Only 500 water molecules are shown.

3.1.2 Hydrophobic Sheets

To model sheets exhibiting different curvatures, we have again placed atoms in a hexagonal pattern with a lattice constant of 1.25 Å. We have studied three systems having sheets with $\kappa = 0$, 0.61, and 1.23 nm^{-1}.

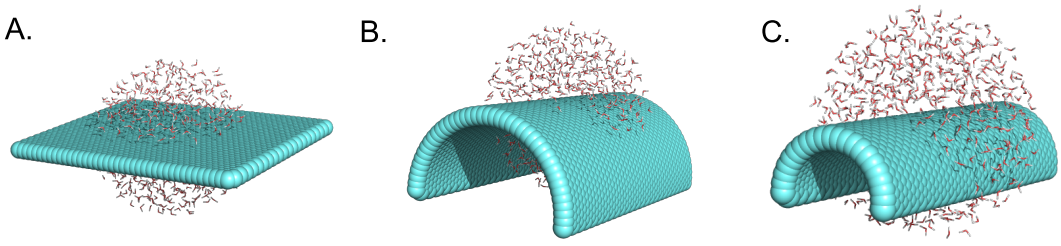

Figure 3.2: Hydrophobic sheets with curvature values ($|\kappa|$): 0 (A), 0.61 (B), and 1.23 (C) nm^{-1} in water.

Sheets having $\kappa = 0$, 0.61, and 1.23 nm^{-1} were solvated with 7920, 4896, and 5061 water molecules. SPC/E water model was used. Lennard-Jones (LJ) parameter $\epsilon = 0.478$ kJ mol^{-1} and $\sigma = 0.3275$ nm was used for the atomic species of these hydrophobic sheets. The flat sheet lay parallel to the xy plane. The length of the curved sheets lies along the z-axis.

3.1.3 Graphene-like Sheets

To model Graphene-like sheets of different curvatures, we have utilized Visual Molecular Dynamics (VMD) [23], a molecular modeling and visualization program. The Nanostructure Builder Plugin allows the construction of single-walled nanotubes and graphene sheets. Thus, we constructed an armchair graphene sheet parallel to the xy plane. Armchair Carbon nanotubes (CNTs) with chiral index (n) = 12 and 24 were also constructed with their length along the z-axis. The CNTs were cut in half to obtain corresponding hCNTS (hemicylindrical carbon nanotubes). The curvatures of the hCNTs with n = 12 and 24 are 0.61, and 1.23 nm^{-1} respectively. Because of the chemical similarity between graphene and hCNTs, these hCNTs may serve as graphene with curvature, $|\kappa| = 0.61$ and 1.23 nm^{-1}.

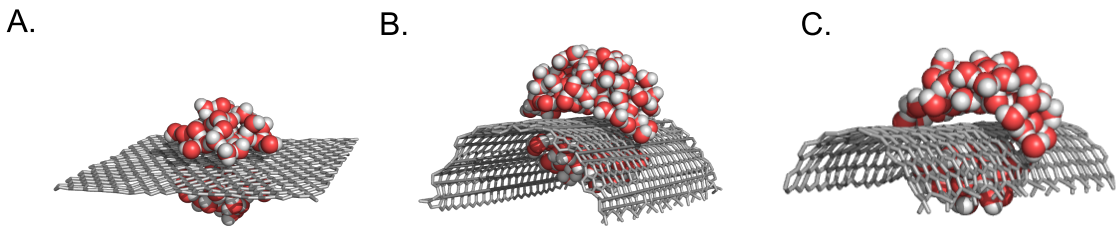

Figure 3.3: Graphene-like sheets with curvature values ($|\kappa|$): 0 (A), 0.61 (B), and 1.23 (C) nm^{-1} in water.

We have described the C-C interactions in the sheet with the AMBER96 force field [24] and the water-water interactions primarily with the rigid SPC/E water model. The number of water molecules ranged from 3421 to 6421. The Lennard-Jones (LJ) parameters for carbon-oxygen interactions are $\sigma_{CO} = 0.3275$ nm and $\epsilon_{CO} = 0.478$ kJ mol^{-1} [25, 26]. To study the effect of hydrophobicities, we have tuned graphene-water interactions, u(r),

using the Weeks-Chandler-Andersen(WCA) scheme [27] as follows:

$$u(r) = \begin{cases} 4\epsilon \left(\left(\frac{\sigma}{r}\right)^{12} - \left(\frac{\sigma}{r}\right)^{6} + \frac{1-\lambda}{4} \right) & : r < 2^{1/6}\sigma \\ 4\epsilon\lambda \left(\left(\frac{\sigma}{r}\right)^{12} - \left(\frac{\sigma}{r}\right)^{6} \right) & : r \geq 2^{1/6}\sigma \end{cases} \tag{3.1}$$

where λ is the scaling factor. $\lambda = 1$ corresponds to the original LJ interactions, while $\lambda = 0$ corresponds to the repulsive WCA potential. So, we have studied each graphene-like sheet with λ=0, 0.5, and 1. Hence, we have studied 9 systems.

3.2 Simulation Details

In all the cases, Molecular Dynamics simulations were performed using GROMACS software package [28]. Energy minimization was performed using the steepest descent algorithm. The energy minimized system was then brought up to 300K using the Berendsen thermostat. Afterward, an NPT equilibration at 300K temperature and 1 bar pressure was performed for 10 ns utilizing the Berendsen thermostat and the Berendsen barostat [29] respectively. The final production run was an NPT simulation 100 ns long using the above-mentioned thermostat and barostat with an integrator timestep of 2fs. Configurations were stored every 5 ps. The slabs, sheets, and hCNTS were kept rigid and fixed throughout the simulation.

3.3 Entropy Calculation

For single water entropy calculations from the MD trajectory, the following steps were followed:

i. We have first ordered the water molecules according to their distance from the model surface. This step is done to reduce the water molecules to be permuted.

ii. Around 500 water molecules around the surface were permuted. Permutation Reduction was performed on individual water molecules by using oxygen-oxygen distance.

iii. Entropy calculations were performed over the permuted trajectory.

iv. Convergence of entropy for each water molecule was checked with time.

3.4 Computing Autocorrelation Functions

To compute the velocity and rotational autocorrelation functions:

i. We run a 20 ps simulation with a well-equilibrated configuration as our initial configuration. We saved the configurations every 4 fs.

ii. As the water molecules change their positions throughout the simulation, we first identified the water molecules that continuously reside within the interface for the total simulation time.

iii. We computed normalized velocity and rotational autocorrelation functions for those water molecules using Gromacs software.

3.5 Proximal Radial Distribution Function

To compute PRDF for water molecules with the sheet as the reference, we utilized Gromacs software. Since the behavior of water is different in both the concave ($\kappa<0$) and convex regions ($\kappa>0$) of the sheet, we computed PRDF for water in both regions separately. In order to do so, we have first identified the water molecules that lie in the concave and convex regions, respectively. Then, we computed PRDF for water molecules in each region using the -surf flag in gmx rdf. We have used the permutated trajectory for PRDF computation so that the water molecules initially in a region remain in the same region.

3.6 Interaction Energy

The interaction energies of water molecules were determined by post-processing the md trajectory with mdrun-rerun in Gromacs software. To minimize the disregard of the long-range interactions in the rerun, the Coulomb and van der Waals distance cut-offs were extended to 2.8 nm.

Chapter 4

Results and Discussion

We have calculated translational and rotational water entropy for:

- Slabs with hydrophobic cavities of different depth-to understand the effect of cavity depth on water entropy.
- Hydrophobic sheets that vary in curvature-to understand the effect of curvature on water entropy.
- Graphene-like sheets, with two cases analyzed separately. Firstly, sheets that vary in interaction potential but have the same curvature. Secondly, sheets that vary in curvature but contain the same interaction potential. Thus, we have studied the effect of hydrophobicity and curvature on water entropy for graphene-like sheets.

4.1 Effect of Cavity

The water entropy calculations were performed for the systems containing slabs with cavities of depth-5 and 10 ÅṪhe entropy values were found to converge with time. The entropy calculations showed an increase in translational entropy inside the cavity. The translational entropy calculated for water molecules as a function of their average distance from the cavity is shown in figure 4.1. Each point in the graph represents the translational entropy of water molecules at a given distance. The TS_{tr} for the individual water molecule inside the cavity was 6.10 and 5.92 kcal mol^{-1} for the cavity of depth-5 and 10 Å, respectively. We can observe from the figure that the translational entropy of all water molecules converges to the bulk entropy value far away from the cavity. The bulk entropy value is around 5.7 kcal mol^{-1}. No significant effect was observed for the rotational entropy of water molecules.

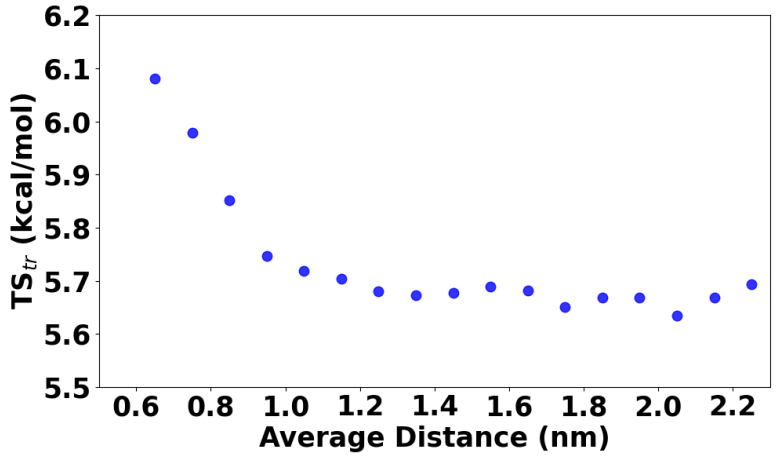

(a)

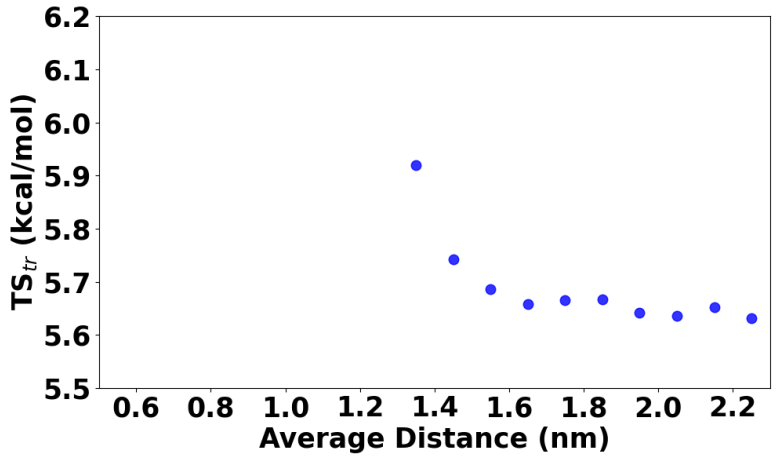

(b)

Figure 4.1: Translational entropy (multiplied by T=300K, TS_{tr}) of individual water molecules as a function of their average distance from the hydrophobic cavity of depth (a) 5 and (b) 10 Å. No point for the initial values of average distance (nm) in both the figures represents the absence of water molecules in that region.

To explain the entropy values, we calculated the interaction energy of water molecules present inside and far away from the cavity. The interaction energy of a water molecule away from the cavity is around -92 kJ mol^{-1}. The interaction energy was found to be -67.90 and -84.26 kJ mol^{-1} for water lying inside the cavity of depth 5 and 10 Å respectively. Therefore, higher entropy inside the cavity and more entropy gain in the cavity of 5 Å depth is due to less negative interaction energy.

4.2 Effect of Curvature

The translational and rotational water entropy were calculated for the systems containing hydrophobic sheets with curvature, $|\kappa|$=0, 0.61, and 1.23 nm^{-1}. The translational and rotational entropy calculated for water molecules as a function of their average distance from the sheet is shown in figure 4.2 and 4.3.

The entropy calculations showed higher translational entropy of the water molecules closest to the sheet, which decreases with the distance from the sheet, finally converging to the bulk value for flat (κ=0 nm^{-1}) and concave regions (κ=-0.61 and -1.23 nm^{-1}). In comparison, the entropy values were less than the bulk value for water in convex regions (κ=0.61 and 1.23 nm^{-1}). Hence, for a particular curvature value ($|\kappa|$), water molecules in the concave region had higher entropy than those in the convex region. Rotational entropy was also higher for the water molecules in the flat and concave regions. The variation of the entropy of the water molecules as a function of curvature is shown in figure 4.4, indicating a decrease in water entropy from concave region (negative curvature) to convex region (positive curvature).

Further, we studied the dynamic behavior of water within the interface. The normalized velocity autocorrelation functions (VACFs) of water molecules within the interface for $|\kappa|$=0, 0.614, and 1.229 nm^{-1} are shown in the figure 4.5. We observed a decrease in the depth of minima in the VACFs for water within the interface. As negative regions in the VACF plots are associated with the reversals of the water molecule's velocity due to collisions with surrounding water; the decrease in depth indicates a less constrained environment. This inference aligns with the decreased coordination numbers of water molecules within the interface, as shown in the table 4.1. The bulk coordination number is approximately 6.6. All the VACFs were found to decorrelate within 0.25 ps. We computed the diffusion coefficient from the VACF, whose values are in the table 4.2. The diffusion coefficient of water in the concave region exceeds the bulk diffusion coefficient, while it is lower in the convex region, indicating higher mobility in the concave region for each curvature. Similar to entropy values, the diffusion coefficient exhibited higher values in the flat and concave regions, but lower values in the convex regions.

To understand the rotational behavior of the water molecules, we computed the rotational autocorrelation function for molecules within the interface. Water molecules in the concave and flat regions rotate faster, which can be observed by the faster decay in the figure 4.5. The regions with faster decay were found to have higher rotational entropy.

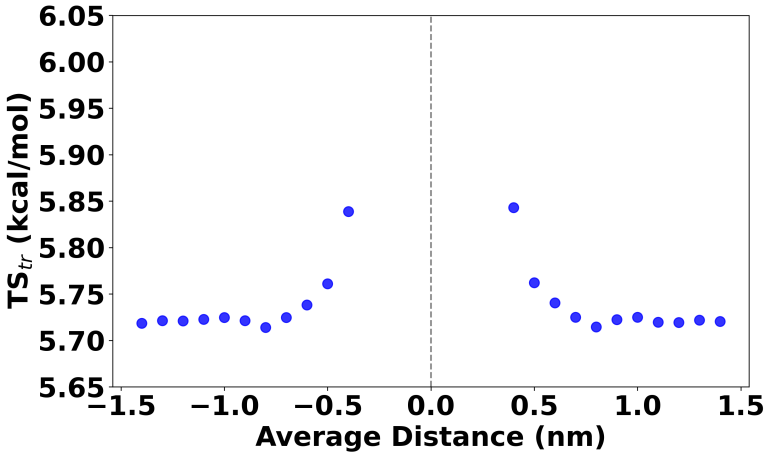

(a)

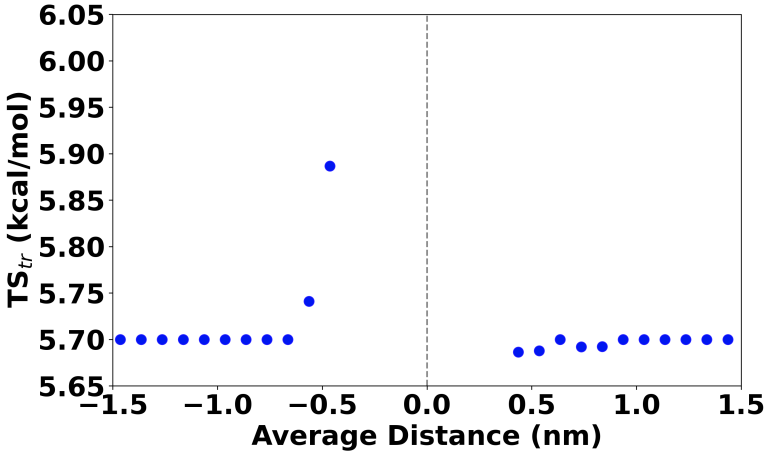

(b)

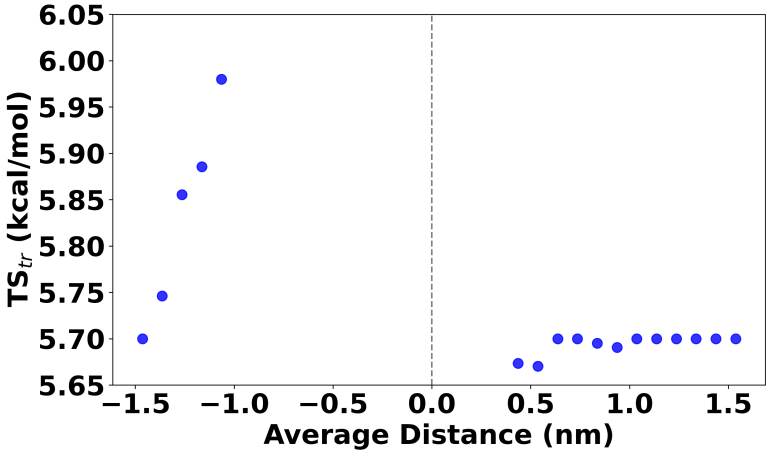

(c)

Figure 4.2: Translational entropy of individual water molecules as a function of their average distance from the hydrophobic sheets of curvature ($|\kappa|$): 0 (a), 0.61 (b), and 1.23 (c) nm^{-1}. The entropy value is multiplied by the temperature, T=300 K. Vertical dashed lines denote the position of the sheet, and the regions with no points denote the absence of water molecules.

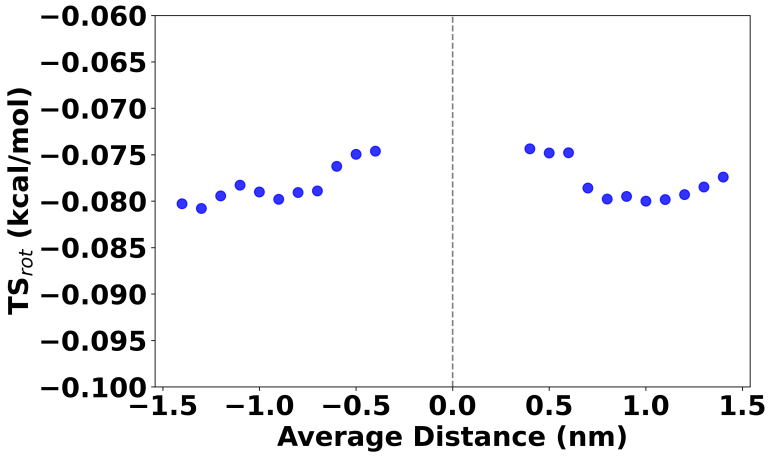

(a)

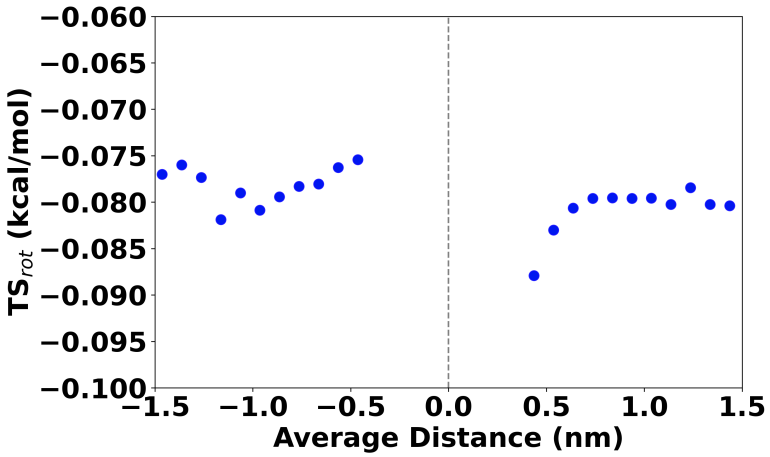

(b)

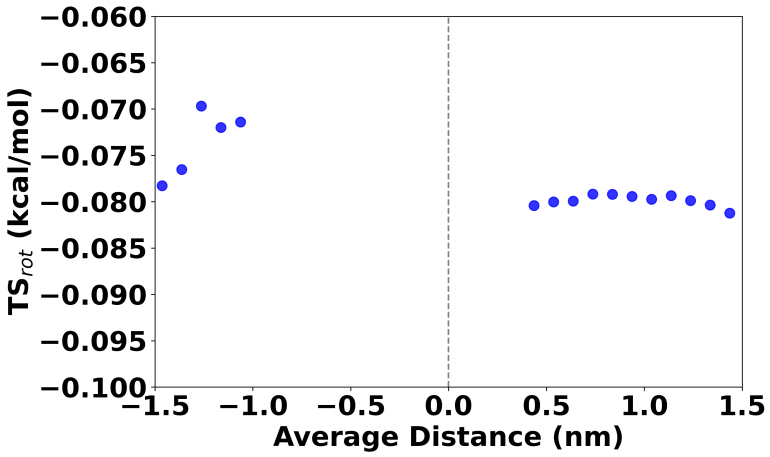

(c)

Figure 4.3: Rotational entropy of individual water molecules as a function of their average distance from the hydrophobic sheets of curvature ($|\kappa|$): 0 (a), 0.61 (b), and 1.23 (c) nm^{-1}. The entropy value is multiplied by the temperature, T=300 K. Vertical dashed lines denote the position of the sheet, and the regions with no points denote the absence of water molecules.

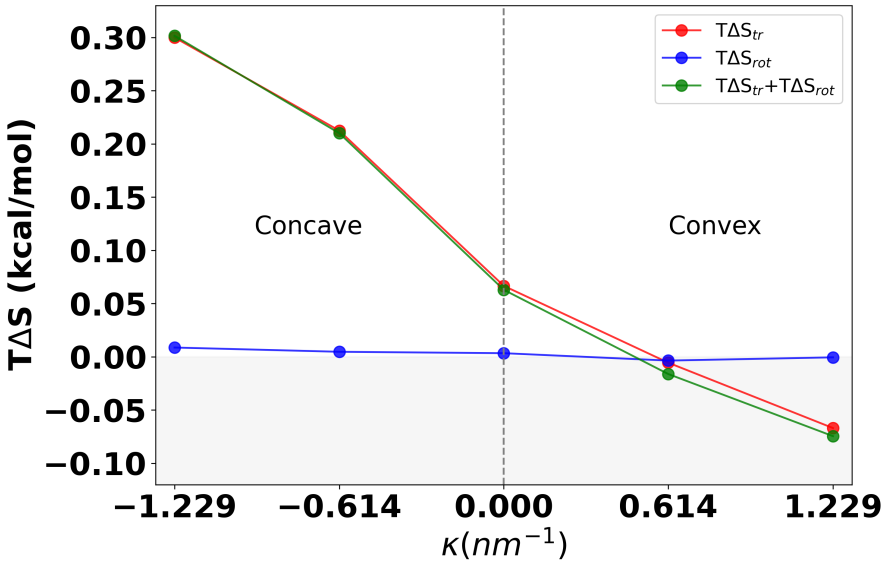

Figure 4.4: Translational, rotational, and total entropy change of individual water molecules in the first hydration layer as a function of the surface curvature, $|\kappa|$. Each point in the shaded region denotes lower water entropy than the bulk value. The convex region is right to the vertical dashed lines, while the concave region is left to the dashed lines.

Table 4.1: Coordination number for water molecules within the interface and bulk for hydrophobic sheets with $|\kappa|$=0, 0.61, and 1.23 nm^{-1}. Across all curvature values, the coordination number within the interface is lower than that in the bulk.

κ (nm^{-1})	Interface	Coordination number
0	Interface	5.38
	Bulk	6.66
0.61	Concave Interface	4.92
	Convex Interface	5.43
	Bulk	6.74
1.23	Concave Interface	5.03
	Convex Interface	5.34
	Bulk	6.66

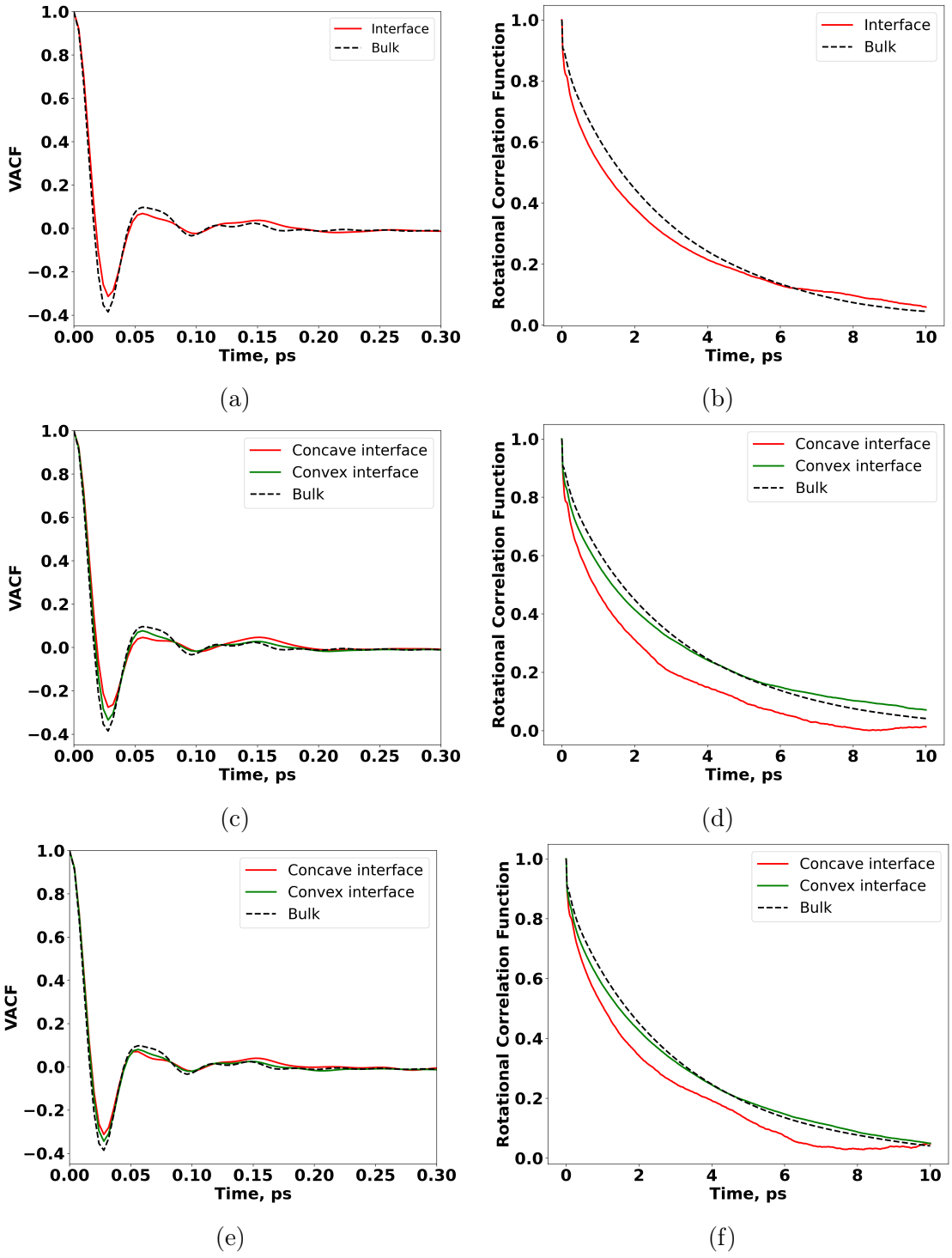

Figure 4.5: Velocity autocorrelation functions (left panel) and Rotational autocorrelation functions (right panel) for water molecules within the interfaces (flat, concave, and convex) as well as in bulk for sheets with curvature, $|\kappa|$=0 (a and b), 0.61 (c and d), and 1.23 (e and f) nm^{-1}.

Table 4.2: Comparison of water diffusion coefficients for sheets with $|\kappa|$=0, 0.61, and 1.23 nm^{-1}. Diffusion coefficients were obtained for water molecules within interfaces (flat, concave, and convex) as well as in the bulk, analyzed over a 20 ps trajectory. The diffusion coefficient increases from the bulk to the flat and concave interfaces. Water within the concave interface has a higher diffusion coefficient than the convex interface.

κ (nm^{-1})	Interface	Diffusion coefficient ($\times 10^{-5}$ cm^2 sec^{-1})
0	Flat	2.26
	Bulk	2.95
0.61	Concave	3.89
	Convex	2.38
	Bulk	2.69
1.23	Concave	3.77
	Convex	2.14
	Bulk	2.85

4.3 Effect of Hydrophobicity and Curvature

We have performed entropy calculations for all the systems containing graphene-like sheets. The translational and rotational entropy of water as a function of its average distance from the sheet is shown in the figure 4.6 and 4.7.

We first investigated the effect of sheet hydrophobicity on water entropy. This involved comparing entropy around sheets with identical curvature (κ) but varying hydrophobicity (λ). Specifically, we studied water entropy surrounding sheets with curvatures of $|\kappa| = 0$, 0.61, and 1.23 nm^{-1}. In all three cases, we observed consistent trends. Sheets with water-sheet interactions corresponding to $\lambda = 0$ exhibited the highest water entropy, followed by $\lambda = 0.5$ and $\lambda = 1.0$. When λ was set to 1, the entropy of the closer water molecule was initially lower, gradually approaching the bulk entropy value. However, for $\lambda = 0$, water entropy was higher near the sheet and decreased gradually to the bulk value. Water entropy was slightly lower near the sheet for intermediate hydrophobicity ($\lambda = 0.5$). We observed that the effect of hydrophobicity was more pronounced for water in the concave regions than in the convex regions.

Next, to understand the effect of the curvature of the sheet on water entropy, we analyzed entropy around sheets with identical hydrophobicity but varying curvatures. We studied three cases, the effect of curvature for λ=0, 0.5, and 1.0. At λ=1.0. water entropy was higher near the convex region, followed by graphene and the concave region. However, at λ=0.5, water entropy near the concave and flat regions exhibited almost

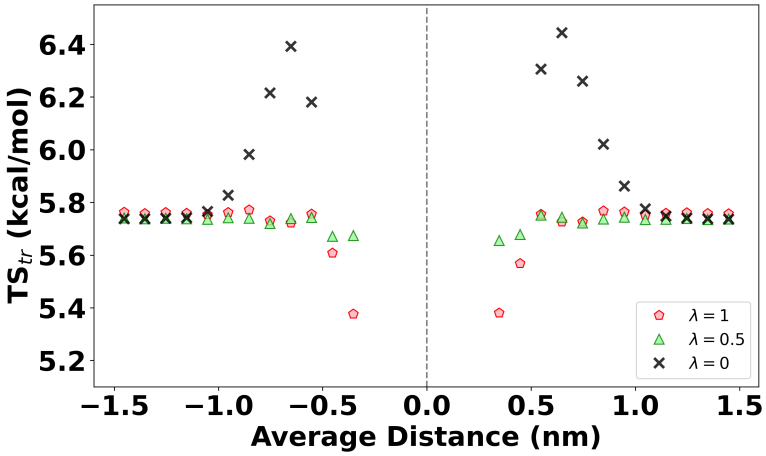

(a)

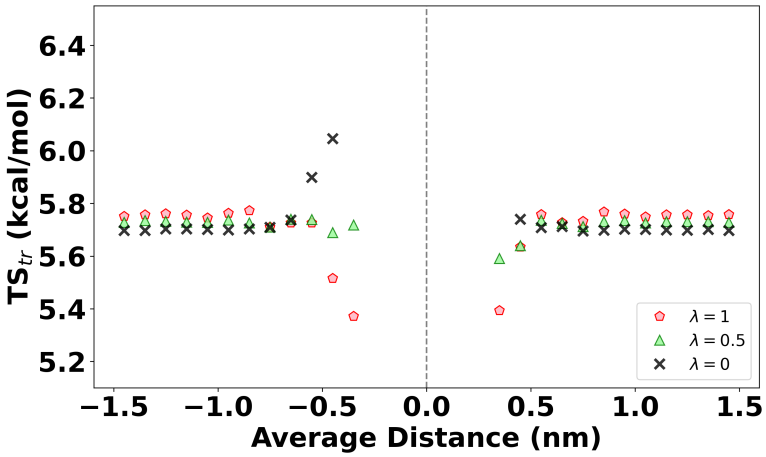

(b)

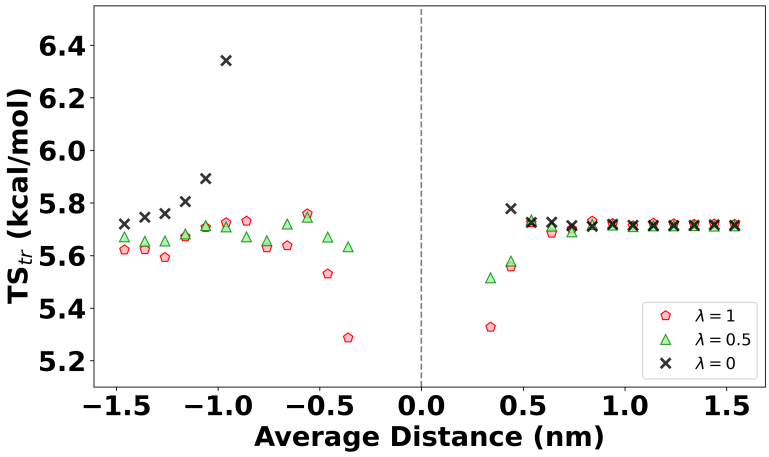

(c)

Figure 4.6: Translational entropy of individual water molecules as a function of their average distance from the graphene-like sheets of curvature ($|\kappa|$): 0 (a), 0.61 (b), and 1.23 (c) nm^{-1}. Each plot shows individual water entropy around sheets having water-sheet interactions corresponding to λ=0, 0.5, and 1.0. The entropy value is multiplied by the temperature of 300 K.

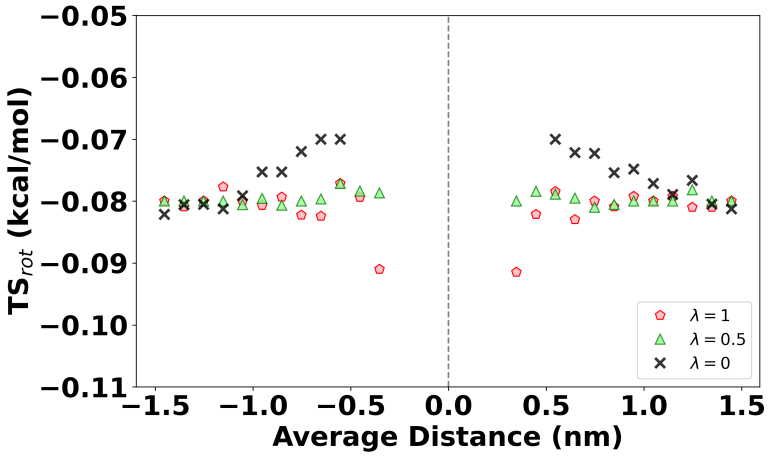

(a)

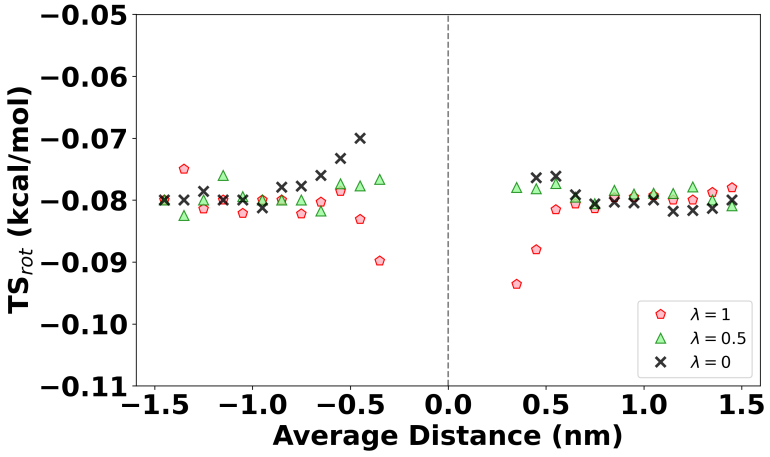

(b)

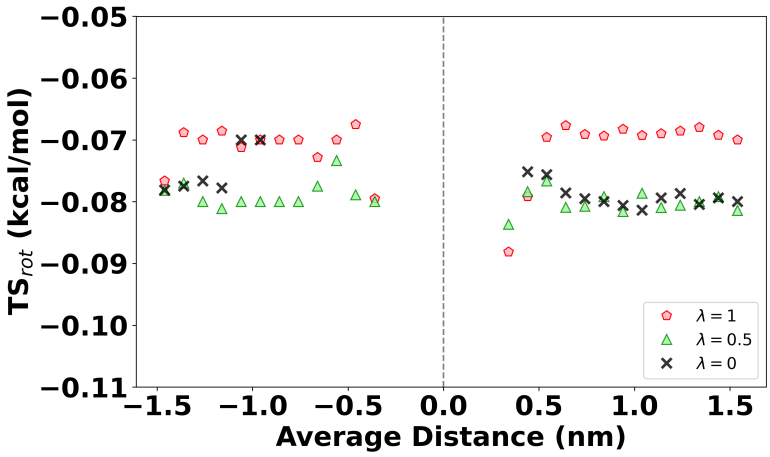

(c)

Figure 4.7: Rotational entropy of individual water molecules as a function of their average distance from the graphene-like sheets of curvature ($|\kappa|$): 0 (a), 0.61 (b), and 1.23 (c) nm^{-1}. Each plot shows individual water entropy around sheets having water-sheet interactions corresponding to λ=0, 0.5, and 1.0. The entropy value is multiplied by the temperature of 300 K.

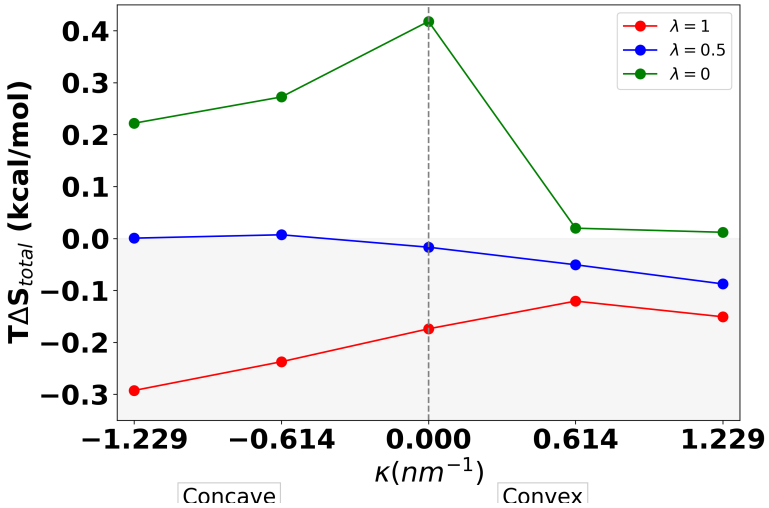

Figure 4.8: Total entropy change of individual water molecules in the first hydration layer as a function of the surface curvature ($|\kappa|$) and hydrophobicity (λ). Each point in the shaded region denotes lower water entropy than the bulk value. Right to the vertical dashed lines is the convex region, while left to the dashed lines is the concave region.

similar values, with the convex region following. Finally, at λ=0, we found that water in the flat region has the highest entropy, followed by the concave and the convex regions. The entropy of water in the first hydration layer as a function of surface curvature and hydrophobicity is shown in figure 4.8; this layer is identified using PRDF, as seen in the figure 4.9.

Further, we computed velocity autocorrelation functions for water molecules within the interface. The normalized VACFs for the water within the interface are shown in the figure 4.10. We can observe the change in the evolution of VACF with an increase in the hydrophobicity. An increase in the hydrophobicity of the sheet results in a decrease in the coordination number of the water molecules within the interface, leading to a decrease in the depth of the minima. When we compared the VACFs for water within the concave and convex regions, greater depth was observed for the VACFs corresponding to the water in the convex region, which is supported by less coordination number in the concave region, as can be seen in the table 4.3. The diffusion coefficient values for water within the interface and in bulk are shown in the table 4.4. The diffusion coefficient was higher for the sheets with λ=0, followed by λ=0.5 and λ=1.0, across all values of κ. When we compared the diffusion coefficient in the concave and convex regions for each system, it was higher in the concave region. So, increasing hydrophobicity results in increased values of both the diffusion coefficient and water entropy. Both entropy and diffusion coefficients are higher in the concave region for λ=0 and 0.5. However, for λ=1.0, although the diffusion coefficient was higher in the concave region, the entropy

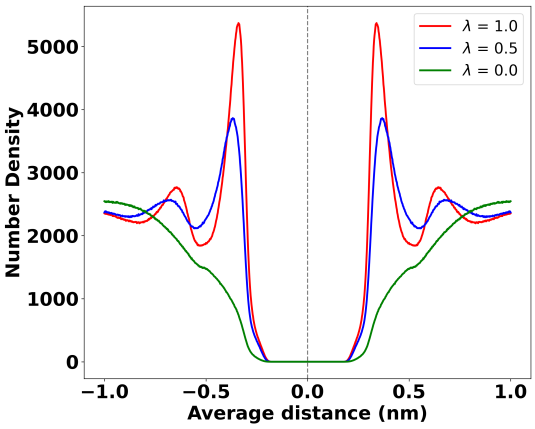

(a)

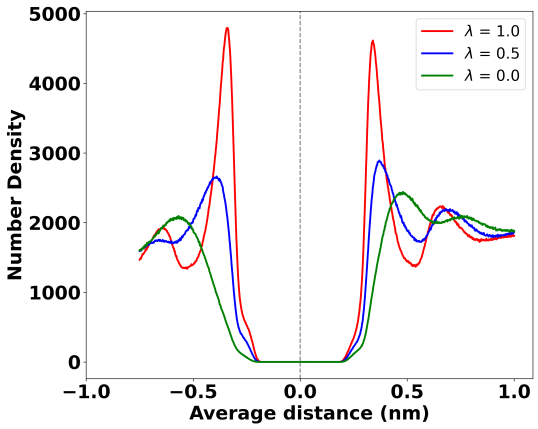

(b)

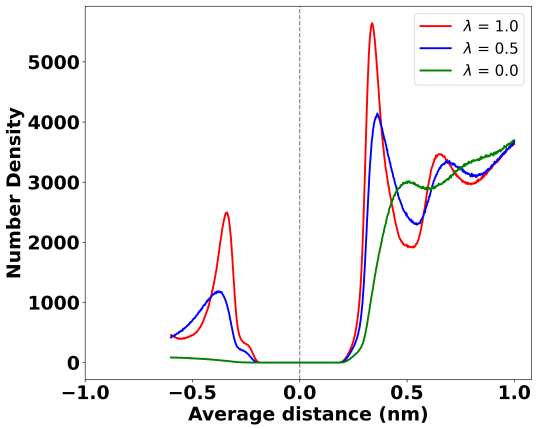

(c)

Figure 4.9: Proximal radial distribution functions for water molecules around graphene-like sheets of curvature, $|\kappa|$: 0 (a), 0.61 (b), and 1.23 (c) nm^{-1}. Each plot shows PRDF for water molecules around sheets having water-sheet interactions corresponding to λ=0, 0.5, and 1.0.

was higher in the convex region.

We also computed the rotational autocorrelation function for water molecules within the interface, as shown in figure 4.11. We observed a faster decay in the correlation function for molecules near sheets having water-sheet interactions corresponding to λ=0, followed by λ=0.5 and λ=0, which aligns with the rotational entropy values. We also compared the rotational correlation functions for water in concave and convex regions and observed a faster decay for water in the concave region. We had observed the same trend for rotational entropy.

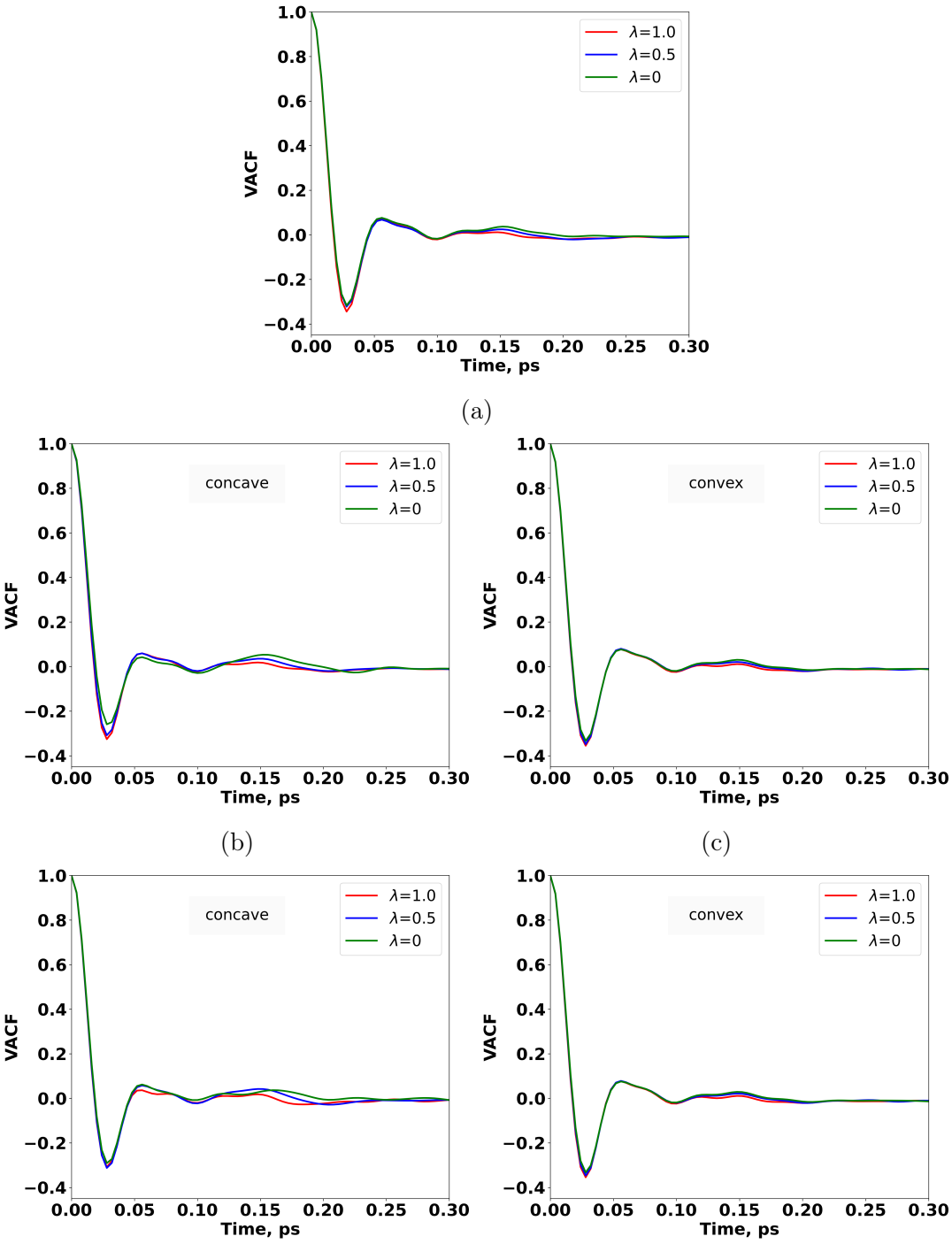

Figure 4.10: Velocity autocorrelation functions for water molecules: (a) within the flat interface for graphene-like sheets with curvature, $|\kappa|$=0 nm^{-1}, (b and c) within concave and convex interface for sheets with curvature, $|\kappa|$= 0.61 nm^{-1}, and (d and e) within concave and convex interface for sheets with curvature, $|\kappa|$=1.23 nm^{-1}. Each plot shows a correlation function for water molecules around sheets having water-sheet interactions corresponding to λ=0, 0.5, and 1.0.

Table 4.3: Coordination number for water molecules within the interface and bulk for sheets having different curvature (κ=0, 0.61, and 1.23 nm^{-1}) and hydrophobicity (λ=0, 0.5, and 1.0). For all the sheets, the coordination number within the interface is lower than that in the bulk.

λ	κ (nm^{-1})	Interface	Coordination number
0	0	Flat	5.06
		Bulk	6.41
	0.61	Concave	4.97
		Convex	5.41
		Bulk	6.91
	1.23	Concave	4.38
		Convex	5.42
		Bulk	6.78
0.5	0	Flat	5.11
		Bulk	6.51
	0.61	Concave	4.99
		Convex	5.26
		Bulk	6.54
	1.23	Concave	5.46
		Convex	5.62
		Bulk	6.82
1.0	0	Flat	5.45
		Bulk	6.25
	0.61	Concave	5.34
		Convex	5.61
		Bulk	6.30
	1.23	Concave	5.54
		Convex	5.77
		Bulk	6.69

Table 4.4: Comparison of water diffusion coefficients for sheets having different curvature (κ=0, 0.61, and 1.23 nm^{-1}) and hydrophobicity (λ=0, 0.5, and 1.0). Diffusion coefficients were obtained for water molecules within interfaces (flat, concave, and convex) and in the bulk, analyzed over a 20 ps trajectory.

λ	κ (nm^{-1})	Interface	Diffusion coefficient ($\times 10^{-5}$ cm^2 sec^{-1})
0	0	Flat	3.38
		Bulk	2.86
	0.61	Concave	3.05
		Convex	1.96
		Bulk	2.50
	1.23	Concave	2.08
		Convex	2.22
		Bulk	2.97
0.5	0	Flat	2.66
		Bulk	2.81
	0.61	Concave	2.20
		Convex	1.56
		Bulk	2.43
	1.23	Concave	1.99
		Convex	1.45
		Bulk	2.67
1.0	0	Flat	1.84
		Bulk	2.49
	0.61	Concave	1.82
		Convex	1.40
		Bulk	2.94
	1.23	Concave	1.60
		Convex	1.55
		Bulk	2.36

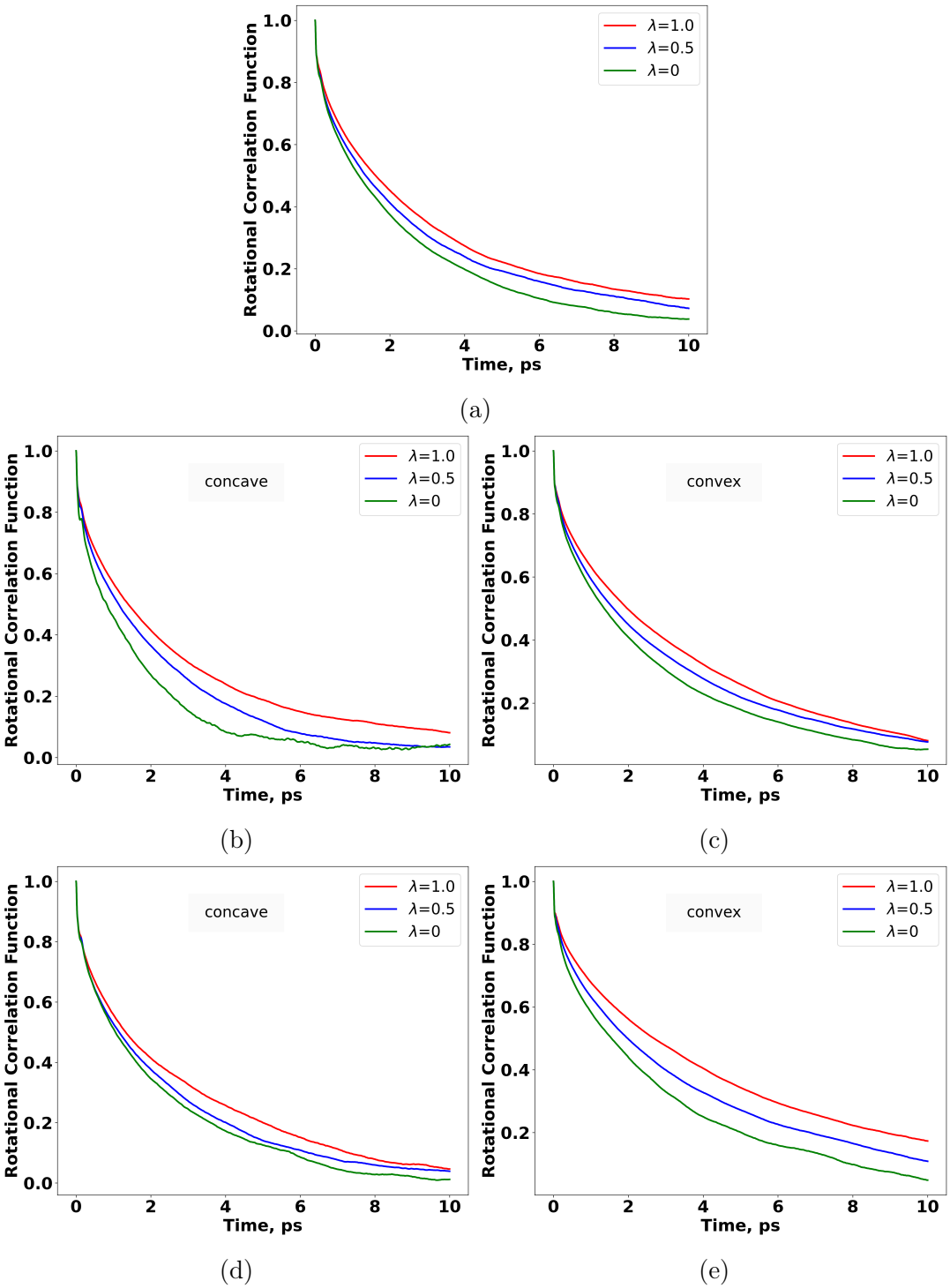

Figure 4.11: Rotational autocorrelation functions for water molecules: (a) within the flat interface for graphene-like sheets with curvature, $|\kappa|$=0 nm^{-1}, (b and c) within concave and convex interface for sheets with curvature, $|\kappa|$= 0.61 nm^{-1}, and (d and e) within concave and convex interface for sheets with curvature, $|\kappa|$=1.23 nm^{-1}. Each plot shows a correlation function for water molecules around sheets having water-sheet interactions corresponding to λ=0, 0.5, and 1.0.

Chapter 5

Conclusion and Future Outlooks

Here, we have applied the Single Water Entropy (SWE) approach to calculate the translational and rotational entropy of water molecules within the cavity and surrounding hydrophobic and graphene-like sheets. We have shown that the water inside the cavity has a higher entropy value than bulk entropy. Water entropy inside the cavity of depth 5 Å was higher compared to water entropy inside the cavity of 10 Å, which can be explained by less negative water-water interaction energy of water inside the cavity of depth 5 Å. We have also studied the effect of curvature on water entropy, showing a decrease in entropy values from negative to positive curvature. Hence, the entropy of water molecules in the concave region is higher than that in the convex region. We have calculated diffusion coefficients and rotational autocorrelation functions that followed the same trend.

Incorporating chemical aspects into our analysis, we calculated water entropy around graphene-like sheets. We have studied sheets with hydrophobicity corresponding to λ=0 (repulsive WCA potential), 0.5, and 1.0 (LJ potential). We have shown that increasing hydrophobicity results in higher entropy for all curvature values. We have observed higher entropy in the concave region for λ= 0 and 0.5, while lower entropy for λ = 1.0. Increasing hydrophobicity also resulted in increase in diffusion coefficient values. Diffusion coefficient was found to be higher in the concave regions for all the λ values. Faster decay of the rotational autocorrelation function for hydrophobic systems aligned with higher rotational entropy.

So, our study was initiated with entropy calculations around model hydrophobic surfaces and extended to incorporate chemical considerations. We could utilize this single water entropy approach to study water entropy around many more model surfaces with varying curvature and surface charge densities. Such studies would enhance our understanding of how these model surfaces influence water entropy, thereby contributing to a deeper understanding of water behavior around macromolecules like proteins.

Bibliography

(1) Ferenczy, G. G.; Kellermayer, M. Contribution of hydrophobic interactions to protein mechanical stability. *Computational and Structural Biotechnology Journal* **2022**, *20*, 1946–1956.

(2) Sriramulu, D. K.; Lee, S.-G. Combinatorial effect of ligand and ligand-binding site hydrophobicities on binding affinity. *J. Chem. Inf. Model.* **2020**, *60*, 1678–1684.

(3) Gorfe, A. A.; Baron, R.; McCammon, J. A. Water-membrane partition thermodynamics of an amphiphilic lipopeptide: an enthalpy-driven hydrophobic effect. *Biophys. J.* **2008**, *95*, 3269–3277.

(4) Galamba, N. Water's structure around hydrophobic solutes and the iceberg model. *J. Phys. Chem. B* **2013**, *117*, 2153–2159.

(5) Davis, J. G.; Gierszal, K. P.; Wang, P.; Ben-Amotz, D. Water structural transformation at molecular hydrophobic interfaces. *Nature* **2012**, *491*, 582–585.

(6) Pascal, T. A.; Goddard 3rd, W. A. Entropic stabilization of water at graphitic interfaces. *J. Phys. Chem. Lett.* **2021**, *12*, 9162–9168.

(7) Saha, D.; Mukherjee, A. Impact of ions on individual water entropy. *J. Phys. Chem. B* **2016**, *120*, 7471–7479.

(8) Peter, C.; Oostenbrink, C.; van Dorp, A.; van Gunsteren, W. F. Estimating entropies from molecular dynamics simulations. *J. Chem. Phys.* **2004**, *120*, 2652–2661.

(9) Lazaridis, T. Inhomogeneous fluid approach to solvation thermodynamics. 1. Theory. *J. Phys. Chem. B* **1998**, *102*, 3531–3541.

(10) Lin, S.-T.; Maiti, P. K.; Goddard 3rd, W. A. Two-phase thermodynamic model for efficient and accurate absolute entropy of water from molecular dynamics simulations. *J. Phys. Chem. B* **2010**, *114*, 8191–8198.

(11) Lin, S.-T.; Blanco, M.; Goddard III, W. A. The two-phase model for calculating thermodynamic properties of liquids from molecular dynamics: Validation for the phase diagram of Lennard-Jones fluids. *J. Chem. Phys.* **2003**, *119*, 11792–11805.

(12) Lazaridis, T. Inhomogeneous fluid approach to solvation thermodynamics. 2. Applications to simple fluids. *J. Phys. Chem. B* **1998**, *102*, 3542–3550.

(13) Heinz, L. P.; Grubmüller, H. Per|Mut: Spatially resolved hydration entropies from atomistic simulations. *J. Chem. Theory Comput.* **2021**, *17*, 2090–2098.

(14) Sasikala, W. D.; Mukherjee, A. Single water entropy: hydrophobic crossover and application to drug binding. *J. Phys. Chem. B* **2014**, *118*, 10553–10564.

(15) Schlitter, J. Estimation of absolute and relative entropies of macromolecules using the covariance matrix. *Chem. Phys. Lett.* **1993**, *215*, 617–621.

(16) Reinhard, F.; Grubmüller, H. Estimation of absolute solvent and solvation shell entropies via permutation reduction. *J. Chem. Phys.* **2007**, *126*, 014102.

(17) Numata, J.; Wan, M.; Knapp, E.-W. In *Genome Informatics 2007*, IMPERIAL COLLEGE PRESS: Institute of Medical Science, University of Tokyo, Japan, 2007.

(18) Lazaridis, T.; Paulaitis, M. E. Entropy of hydrophobic hydration: a new statistical mechanical formulation. *J. Phys. Chem.* **1992**, *96*, 3847–3855.

(19) Taylor, G. I. DIFFUSION B CONTINUOU MOVEMENT, `https://courses.washington.edu/mengr537/Lecture_Notes/DiffusionContinuousMovements_TaylorDispersion_ProcMathSocLon1921.pdf`, Accessed: 2024-3-28.

(20) Green, M. S. Markoff random processes and the statistical mechanics of time-dependent phenomena. II. Irreversible processes in fluids. *J. Chem. Phys.* **1954**, *22*, 398–413.

(21) Kubo, R. Statistical-mechanical theory of irreversible processes. I. general theory and simple applications to magnetic and conduction problems. *J. Phys. Soc. Jpn.* **1957**, *12*, 570–586.

(22) Berendsen, H. J. C.; Grigera, J. R.; Straatsma, T. P. The missing term in effective pair potentials. *J. Phys. Chem.* **1987**, *91*, 6269–6271.

(23) Humphrey, W.; Dalke, A.; Schulten, K. VMD – Visual Molecular Dynamics. *Journal of Molecular Graphics* **1996**, *14*, 33–38.

(24) Cornell, W. D.; Cieplak, P.; Bayly, C. I.; Gould, I. R.; Merz, K. M.; Ferguson, D. M.; Spellmeyer, D. C.; Fox, T.; Caldwell, J. W.; Kollman, P. A. A second generation force field for the simulation of proteins, nucleic acids, and organic molecules. *J. Am. Chem. Soc.* **1995**, *117*, 5179–5197.

(25) Hummer, G.; Rasaiah, J. C.; Noworyta, J. P. Water conduction through the hydrophobic channel of a carbon nanotube. *Nature* **2001**, *414*, 188–190.

(26) Kalra, A.; Garde, S.; Hummer, G. Osmotic water transport through carbon nanotube membranes. *Proc. Natl. Acad. Sci. U. S. A.* **2003**, *100*, 10175–10180.

(27) Weeks, J. D.; Chandler, D.; Andersen, H. C. Role of repulsive forces in determining the equilibrium structure of simple liquids. *J. Chem. Phys.* **1971**, *54*, 5237–5247.

(28) Lindahl; Abraham; Hess; Spoel, V. d. GROMACS 2021.4 Source code, 2021.

(29) Berendsen, H. J. C.; Postma, J. P. M.; van Gunsteren, W. F.; DiNola, A.; Haak, J. R. Molecular dynamics with coupling to an external bath. *J. Chem. Phys.* **1984**, *81*, 3684–3690.